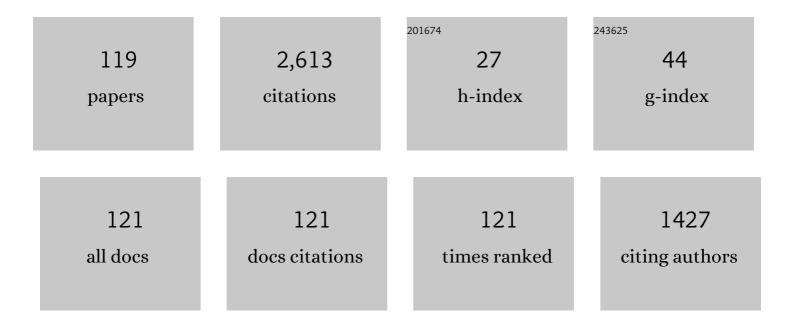
Jiang Wang

List of Publications by Year in descending order

Source: https://exaly.com/author-pdf/10213931/publications.pdf Version: 2024-02-01



LIANC WANC

#	Article	IF	CITATIONS
1	Magnetic properties and giant cryogenic magnetocaloric effect in B-site ordered antiferromagnetic Gd2MgTiO6 double perovskite oxide. Acta Materialia, 2022, 226, 117669.	7.9	131
2	Magnetic properties and promising magnetocaloric performances in the antiferromagnetic GdFe2Si2 compound. Science China Materials, 2022, 65, 1345-1352.	6.3	116
3	Mechanical and inÂvitro study of an isotropic Ti6Al4V lattice structure fabricated using selective laser melting. Journal of Alloys and Compounds, 2019, 782, 209-223.	5.5	112

Structure, magnetic properties and cryogenic magneto-caloric effect (MCE) in RE2FeAlO6 (RE = Gd, Dy,) Tj ETQq0 0.0 rgBT /Overlock 10 $\frac{100}{105}$

5	Effect of scanning speed on the microstructure and mechanical behavior of 316L stainless steel fabricated by selective laser melting. Materials and Design, 2020, 186, 108355.	7.0	99
6	Achievement of giant cryogenic refrigerant capacity in quinary rare-earths based high-entropy amorphous alloy. Journal of Materials Science and Technology, 2022, 102, 66-71.	10.7	95
7	Study of pore defect and mechanical properties in selective laser melted Ti6Al4V alloy based on X-ray computed tomography. Materials Science & Engineering A: Structural Materials: Properties, Microstructure and Processing, 2020, 797, 139981.	5.6	87
8	Effect of hot isostatic pressing (HIP) on microstructure and mechanical properties of Ti6Al4V alloy fabricated by cold spray additive manufacturing. Additive Manufacturing, 2019, 27, 595-605.	3.0	82
9	Microstructural and mechanical properties of high-performance Inconel 718 alloy by cold spraying. Journal of Alloys and Compounds, 2019, 792, 456-467.	5.5	75
10	First- and second-order phase transitions in RE6Co2Ga (RE = Ho, Dy or Gd) cryogenic magnetocaloric materials. Science China Materials, 2021, 64, 2846-2857.	6.3	62
11	Structure and cryogenic magnetic properties in Ho2BaCuO5 cuprate. Ceramics International, 2018, 44, 1991-1994.	4.8	58
12	Effect of magnetic field on electroplating Ni/nano-Al2O3 composite coating. Journal of Electroanalytical Chemistry, 2009, 630, 42-48.	3.8	57
13	Low field induced large magnetic entropy change in the amorphousized Tm60Co20Ni20 ribbon. Journal of Alloys and Compounds, 2018, 733, 40-44.	5.5	57
14	Study of the microstructure and mechanical performance of C-X stainless steel processed by selective laser melting (SLM). Materials Science & Engineering A: Structural Materials: Properties, Microstructure and Processing, 2020, 781, 139227.	5.6	57
15	Influence of dc electric current on the hardness of thermally aged Cu–Cr–Zr alloy. Journal of Alloys and Compounds, 2009, 479, 303-306.	5.5	54
16	Laser additive manufacturing and homogeneous densification of complicated shape SiC ceramic parts. Ceramics International, 2018, 44, 21067-21075.	4.8	52
17	Rheological behavior of titania ink and mechanical properties of titania ceramic structures by 3D direct ink writing using high solid loading titania ceramic ink. Journal of Alloys and Compounds, 2019, 783, 321-328.	5.5	47
18	Synchrotron tomographic quantification of the influence of Zn concentration on dendritic growth in Mg-Zn alloys. Acta Materialia, 2018, 156, 287-296.	7.9	46

2

#	Article	IF	CITATIONS
19	Selective laser melting of WC reinforced maraging steel 300: Microstructure characterization and tribological performance. Surface and Coatings Technology, 2019, 371, 355-365.	4.8	44
20	Magnetic properties and promising cryogenic magneto-caloric performances of Gd ₂₀ Ho ₂₀ Tm ₂₀ Cu ₂₀ Ni ₂₀ amorphous ribbons*. Chinese Physics B, 2021, 30, 017501.	1.4	40
21	Thermoelectric Magnetohydrodynamic Flows and Their Induced Change of Solid–Liquid Interface Shape in Static Magnetic Field-Assisted Directional Solidification. Metallurgical and Materials Transactions A: Physical Metallurgy and Materials Science, 2016, 47, 1169-1179.	2.2	37
22	Cold spray additive manufacturing of Invar 36 alloy: microstructure, thermal expansion and mechanical properties. Journal of Materials Science and Technology, 2021, 72, 39-51.	10.7	37
23	Refinement of primary Si in the bulk solidified Al-20Âwt.%Si alloy assisting by high static magnetic field and phosphorus addition. Journal of Alloys and Compounds, 2017, 714, 39-46.	5.5	32
24	Cryogenic magnetic properties and magnetocaloric effects (MCE) in B-site disordered RE2CuMnO6 (RE) Tj ETQqQ) 0 0 rgBT 4.8	/Qverlock 10
25	Enhanced mechanical properties of Ti6Al4V alloy fabricated by laser additive manufacturing under static magnetic field. Materials Research Letters, 2022, 10, 530-538.	8.7	31
26	Refinement and growth enhancement of Al2Cu phase during magnetic field assisting directional solidification of hypereutectic Al-Cu alloy. Scientific Reports, 2016, 6, 24585.	3.3	30
27	Microstructure evolution and mechanical properties of maraging steel 300 fabricated by cold spraying. Materials Science & Engineering A: Structural Materials: Properties, Microstructure and Processing, 2019, 743, 482-493.	5.6	29
28	Gelcasting of zirconia-based all-ceramic teeth combined with stereolithography. Ceramics International, 2018, 44, 21556-21563.	4.8	28
29	Modification of liquid/solid interface shape in directionally solidifying Al–Cu alloys by a transverse magnetic field. Journal of Materials Science, 2013, 48, 213-219.	3.7	27
30	Effect of substrate cooling on the epitaxial growth of Ni-based single-crystal superalloy fabricated by direct energy deposition. Journal of Materials Science and Technology, 2021, 62, 148-161.	10.7	26
31	Interfacial metal/ceramic bonding mechanism for metallization of ceramics via cold spraying. Journal of Materials Processing Technology, 2021, 288, 116845.	6.3	25
32	A novel approach to in-situ produce functionally graded silicon matrix composite materials by selective laser melting. Composite Structures, 2017, 172, 251-258.	5.8	23
33	Cold sprayed WC reinforced maraging steel 300 composites: Microstructure characterization and mechanical properties. Journal of Alloys and Compounds, 2019, 785, 499-511.	5.5	23
34	Effect of a high magnetic field on the microstructures in directionally solidified Zn–Cu peritectic alloys. Acta Materialia, 2014, 73, 83-96.	7.9	22
35	Magnetic properties and magnetocaloric effect in the aluminide RE NiAl 2 (RE Â=ÂHo and Er) compounds. Intermetallics, 2017, 88, 61-64.	3.9	21

36Controlling droplet distribution using thermoelectric magnetic forces during bulk solidification
processing of a Zn–6 wt.%Bi immiscible alloy. Materials and Design, 2016, 100, 168-174.7.020

#	Article	IF	CITATIONS
37	The effect of static magnetic field on solid–liquid interfacial free energy of Al–Cu alloy system. Scripta Materialia, 2020, 187, 232-236.	5.2	20
38	Interfacial microstructure of partial transient liquid phase bonding of Si 3 N 4 to nickel-base superalloy using Ti/Au/Ni interlayers. Vacuum, 2016, 130, 105-108.	3.5	18
39	Columnar-to-Equiaxed Transition and Equiaxed Grain Alignment in Directionally Solidified Ni3Al Alloy Under an Axial Magnetic Field. Metallurgical and Materials Transactions A: Physical Metallurgy and Materials Science, 2017, 48, 4193-4203.	2.2	18
40	Enhanced high temperature elongation of nickel based single crystal superalloys by hot isostatic pressing. Journal of Alloys and Compounds, 2019, 805, 78-83.	5.5	18
41	Three dimensional dendritic morphology and orientation transition induced by high static magnetic field in directionally solidified Al-10 wt.%Zn alloy. Journal of Materials Science and Technology, 2019, 35, 1587-1592.	10.7	18
42	Effects of carbon content on microstructure and mechanical properties of SiC ceramics fabricated by SLS/RMI composite process. Ceramics International, 2020, 46, 22015-22023.	4.8	18
43	Revealing the influence of high magnetic field on the solute distribution during directional solidification of Al-Cu alloy. Journal of Materials Science and Technology, 2021, 88, 226-232.	10.7	18
44	Strength-ductility synergy of CoCrNi medium-entropy alloy processed with laser powder bed fusion. Materials and Design, 2022, 219, 110774.	7.0	18
45	Effect of high static magnetic field on the microstructure and mechanical properties of directionally solidified alloy 2024. Journal of Alloys and Compounds, 2018, 749, 978-989.	5.5	17
46	Improvement of tribological performance by micro-arc oxidation treatment on selective laser melting Ti6Al4V alloy. Materials Research Express, 2019, 6, 096509.	1.6	17
47	In-situ observation of solid-liquid interface transition during directional solidification of Al-Zn alloy via X-ray imaging. Journal of Materials Science and Technology, 2020, 39, 113-123.	10.7	17
48	Effect of final electromagnetic stirring on solidification microstructure of GCr15 bearing steel in simulated continuous casting. Journal of Iron and Steel Research International, 2020, 27, 141-147.	2.8	17
49	Evolution of microsegregation in directionally solidified Al–Cu alloys under steady magnetic field. Journal of Alloys and Compounds, 2019, 800, 41-49.	5.5	16
50	Electrical and mechanical properties of Cu–Cr–Zr alloy aged under imposed direct continuous current. Transactions of Nonferrous Metals Society of China, 2012, 22, 1106-1111.	4.2	15
51	Grain Refinement During Directionally Solidifying GCr18Mo Steel at Low Pulling Speeds Under an Axial Static Magnetic Field. Acta Metallurgica Sinica (English Letters), 2018, 31, 681-691.	2.9	15
52	Effect of a constant laser energy density on the evolution of microstructure and mechanical properties of NiTi shape memory alloy fabricated by laser powder bed fusion. Optics and Laser Technology, 2022, 152, 108182.	4.6	15
53	Investigation on microstructure and creep properties of nickel based single crystal superalloys PWA1483 during heat treatment under an alternating magnetic field. Materials Science & Engineering A: Structural Materials: Properties, Microstructure and Processing, 2019, 762, 138087.	5.6	14
54	Compression properties enhancement of Al-Cu alloy solidified under a 29†T high static magnetic field. Materials Science & Engineering A: Structural Materials: Properties, Microstructure and Processing, 2018, 733, 170-178.	5.6	13

#	Article	IF	CITATIONS
55	Pore-scale modeling of wettability effects on infiltration behavior in liquid composite molding. Physics of Fluids, 2020, 32, 093311.	4.0	13
56	Toward Φ56 mm Al-Polar AlN Single Crystals Grown by the Homoepitaxial PVT Method. Crystal Growth and Design, 2022, 22, 3462-3470.	3.0	13
57	Effect of interdendritic thermoelectric magnetic convection on evolution of tertiary dendrite during directional solidification. Journal of Crystal Growth, 2016, 439, 66-73.	1.5	12
58	Tribological properties of Al/diamond composites produced by cold spray additive manufacturing. Additive Manufacturing, 2020, 36, 101434.	3.0	12
59	4D synchrotron X-ray tomographic study of the influence of transverse magnetic field on iron intermetallic compounds precipitation behavior during solidification of Al–Si–Fe alloy. Intermetallics, 2022, 143, 107471.	3.9	12
60	Effects of Electromagnetic Vibration Frequencies on Microstructure and Tensile Properties of Al-15 Wt Pct Sn Alloy in Semi-continuous Casting Process. Metallurgical and Materials Transactions A: Physical Metallurgy and Materials Science, 2017, 48, 3377-3388.	2.2	11
61	Solute trapping in Al-Cu alloys caused by a 29 Tesla super high static magnetic field. Scientific Reports, 2019, 9, 266.	3.3	11
62	Effects of a High Magnetic Field on the Microstructure of Ni-Based Single-Crystal Superalloys During Directional Solidification. Metallurgical and Materials Transactions A: Physical Metallurgy and Materials Science, 2017, 48, 3804-3813.	2.2	10
63	Mechanism of Desulfurization from Liquid Iron by Hydrogen Plasma Arc Melting. Metallurgical and Materials Transactions B: Process Metallurgy and Materials Processing Science, 2018, 49, 2951-2955.	2.1	10
64	Droplet Evolution and Refinement During Liquid–Liquid Decomposition of Zn-6ÂWtÂPct Bi Immiscible Alloy Under High Static Magnetic Fields. Metallurgical and Materials Transactions A: Physical Metallurgy and Materials Science, 2018, 49, 3333-3345.	2.2	10
65	Microstructure and Mechanical Properties of Ni-based Superalloy K418 Produced by the Continuous Unidirectional Solidification Process. Journal of Materials Engineering and Performance, 2019, 28, 6483-6491.	2.5	10
66	Enhanced creep properties of nickel-base single crystal superalloy CMSX-4 by high magnetic field. Materials Science & Engineering A: Structural Materials: Properties, Microstructure and Processing, 2021, 803, 140729.	5.6	10
67	Motion of Solid Grains During Magnetic Field-Assisted Directional Solidification. Metallurgical and Materials Transactions B: Process Metallurgy and Materials Processing Science, 2018, 49, 861-865.	2.1	9
68	Effect of Static Magnetic Field on the Evolution of Residual Stress and Microstructure of Laser Remelted Inconel 718 Superalloy. Journal of Thermal Spray Technology, 2020, 29, 1410-1423.	3.1	9
69	Microstructure and mechanical properties of directionally solidified Al-rich Ni3Al-based alloy under static magnetic field. Journal of Materials Science and Technology, 2022, 110, 117-127.	10.7	9
70	Homogeneous Hypermonotectic Alloy Fabricated by Electric-Magnetic-Compound Field Assisting Solidification. Materials Today: Proceedings, 2015, 2, S364-S372.	1.8	8
71	Enhanced undercooling of para- and diamagnetic metal melts in steady magnetic field. Japanese Journal of Applied Physics, 2018, 57, 080301.	1.5	8
72	Effect of a High Static Magnetic Field on the Origin of Stray Grains during Directional Solidification. Materials Transactions, 2016, 57, 1230-1235.	1.2	7

#	Article	IF	CITATIONS
73	Effect of a high magnetic field on solidification structure in directionally solidified NiAl-Cr(Mo)-Hf eutectic alloy. Journal of Alloys and Compounds, 2018, 737, 74-82.	5.5	7
74	Thermal and numerical simulation of mould electromagnetic stirring of GCr15 bearing steel. Materials Science and Technology, 2019, 35, 2173-2180.	1.6	7
75	Effects of substrate heat accumulation on the cold sprayed Ni coating quality: Microstructure evolution and tribological performance. Surface and Coatings Technology, 2019, 371, 185-193.	4.8	7
76	Manganese Removal from Liquid Nickel by Hydrogen Plasma Arc Melting. Materials, 2019, 12, 33.	2.9	7
77	Table-like shape magnetocaloric effect and large refrigerant capacity in dual-phase HoNi/HoNi ₂ composite*. Chinese Physics B, 2020, 29, 107502.	1.4	7
78	Effects of Static Magnetic Field on the Microstructure of Selective Laser Melted Inconel 625 Superalloy: Numerical and Experiment Investigations. Metals, 2021, 11, 1846.	2.3	7
79	Microstructure evolution and room temperature fracture toughness of directionally solidified NiAl–31Cr3Mo–0.2Si near-eutectic alloy at different withdrawal rates. Materials Science & Engineering A: Structural Materials: Properties, Microstructure and Processing, 2016, 678, 243-251.	5.6	6
80	Effect of a high magnetic field on the microstructure in directionally solidified two-phase Ni3Al alloys. Materials Letters, 2017, 189, 131-135.	2.6	6
81	Investigation of Thermo-Electro-Magnetic force on equiaxed grain motion during upward directional solidification. International Journal of Thermal Sciences, 2019, 145, 106047.	4.9	6
82	Enhanced Dendrite Coarsening and Microsegregation in Al–Cu Alloy under a Steady Magnetic Field. Materials Transactions, 2019, 60, 1921-1927.	1.2	6
83	Influence of static magnetic field on the heterogeneous nucleation behavior of Al on single crystal Al2O3 substrate. Materialia, 2020, 13, 100847.	2.7	6
84	Application of Heat Absorption Method to Improve Quality of Large Steel Ingot. ISIJ International, 2021, 61, 865-870.	1.4	6
85	Establishment of constitutive models and numerical simulation of dry pressing and solid state sintering processes of MgTiO3 ceramic. Ceramics International, 2021, 47, 8769-8780.	4.8	6
86	In-situ nitrogen strengthening of selective laser melted Ti6Al4V with superior mechanical performance. Additive Manufacturing, 2021, 46, 102142.	3.0	6
87	Application of Synchrotron X-Ray Imaging and Diffraction in Additive Manufacturing: A Review. Acta Metallurgica Sinica (English Letters), 2022, 35, 25-48.	2.9	6
88	On the role of volumetric energy density in the microstructure and mechanical properties of laser powder bed fusion Ti-6Al-4V alloy. Additive Manufacturing, 2022, 51, 102605.	3.0	6
89	Application of heat absorption method to reduce macrosegregation during solidification of bearing steel ingot. Journal of Iron and Steel Research International, 2022, 29, 1915-1926.	2.8	6
90	Microstructure evolution and mechanical properties of laser additive manufactured Ti6Al4V alloy under nitrogen-argon reactive atmosphere. Materials Science & Engineering A: Structural Materials: Properties, Microstructure and Processing, 2022, 841, 143076.	5.6	6

#	Article	IF	CITATIONS
91	Evolution of microstructure and mechanical property of Ti-47Al-2Cr-2Nb intermetallic alloy by laser direct energy deposition: From a single-track, thin-wall to bulk. Materials Characterization, 2022, 190, 112053.	4.4	6
92	Magnetic Fields, Convection and Solidification. Materials Science Forum, 0, 790-791, 375-383.	0.3	5
93	Effect of a transverse magnetic field on the growth of equiaxed grains during directional solidification. Materials Letters, 2015, 161, 595-600.	2.6	5
94	Reduction in Microsegregation in Al–Cu Alloy by Alternating Magnetic Field. Acta Metallurgica Sinica (English Letters), 2020, 33, 267-274.	2.9	5
95	Loading of Zn/ZnO particles in the precursor feedstock affects the characteristics of liquid plasma sprayed nano-ZnO coatings for photocatalytic applications. Nanotechnology, 2020, 31, 185301.	2.6	5
96	Revealing the Diversity of Dendritic Morphology Evolution During Solidification of Magnesium Alloys using Synchrotron X-ray Imaging: A Review. Acta Metallurgica Sinica (English Letters), 2022, 35, 177-200.	2.9	5
97	Effect of annealing treatment on microstructure and mechanical properties of cold sprayed TiB2/AlSi10Mg composites. Surfaces and Interfaces, 2021, 26, 101341.	3.0	5
98	Glass forming ability, magnetic properties and cryogenic magnetocaloric effects in RE60Co20Al20 (REÂ=ÂHo, Er, Tm) amorphous ribbons. Journal of Alloys and Compounds, 2022, 895, 162633.	5.5	5
99	Selective Laser Melting of Carbon-Free Mar-M509 Co-Based Superalloy: Microstructure, Micro-Cracks, and Mechanical Anisotropy. Acta Metallurgica Sinica (English Letters), 2022, 35, 501-516.	2.9	5
100	Effect of steady magnetic field on undercooling of Al-Cu alloy melts. Europhysics Letters, 2019, 126, 46001.	2.0	4
101	Orientation and alignment during materials processing under high magnetic fields. Chinese Physics B, 2019, 28, 048301.	1.4	4
102	Enhanced Degradation in Grain Refinement of Inoculated 2024 Al Alloy in Steady Magnetic field. Metallurgical and Materials Transactions A: Physical Metallurgy and Materials Science, 2020, 51, 4584-4591.	2.2	4
103	3D actual microstructure-based modeling of non-isothermal infiltration behavior and void formation in liquid composite molding. Applied Mathematical Modelling, 2021, 94, 388-402.	4.2	4
104	Influences of Powder Source Porosity on Mass Transport during AlN Crystal Growth Using Physical Vapor Transport Method. Crystals, 2021, 11, 1436.	2.2	4
105	Effects of laser scanning speed and building direction on the microstructure and mechanical properties of selective laser melted Inconel 718 superalloy. Materials Today Communications, 2022, 30, 103095.	1.9	4
106	Cell-to-Dendrite Transition Induced by a Static Transverse Magnetic Field During Lasering Remelting of the Nickel-Based Superalloy. Metallurgical and Materials Transactions B: Process Metallurgy and Materials Processing Science, 2018, 49, 3211-3219.	2.1	3
107	Effect of Thermoelectric Magnetic Convection on Shrinkage Porosity at the Final Stage of Solidification of GCr18Mo Steel Under Axial Static Magnetic Field. Metallurgical and Materials Transactions B: Process Metallurgy and Materials Processing Science, 2019, 50, 881-889.	2.1	3
108	Magnetic-Field-Induced Liquid–Solid Interface Transformation and Its Effect on Microsegregation in Directionally Solidified Ni-Cr Alloy. Metallurgical and Materials Transactions A: Physical Metallurgy and Materials Science, 2020, 51, 4592-4601.	2.2	3

#	Article	IF	CITATIONS
109	Objective evaluation of wearable thermoelectric generator: From platform building to performance verification. Review of Scientific Instruments, 2022, 93, 045105.	1.3	3
110	<i>In Situ</i> and Real-Time Analysis of TEM Forces Induced by a Permanent Magnetic Field during Solidification of Al-4wt%Cu. Materials Science Forum, 0, 790-791, 420-425.	0.3	2
111	Effects of Y addition on the microstructure and properties of Cu-Cr-Zr alloy during the directional solidification process. Materials Research Express, 2018, 5, 116505.	1.6	2
112	Effect of annealing treatment on the microstructure and mechanical properties of Fe-18Mn-0.8C-0.2 V TWIP steel. Materials Research Express, 2019, 6, 1265h4.	1.6	2
113	Effect of Spheroidizing Annealing in Combination with Alternating Magnetic Field on Microstructure and Mechanical Properties of GCr15 Bearing Steel. ISIJ International, 2022, 62, 1275-1282.	1.4	2
114	High-magnetic-field-induced formation of aligned equiaxed grains during directional solidification. Philosophical Magazine Letters, 2015, 95, 425-432.	1.2	1
115	Numerical simulation and experimental verification of dry pressed MgTiO ₃ ceramic body during pressureless sintering. Journal of the American Ceramic Society, 2021, 104, 4408-4419.	3.8	1
116	The influence of a magnet field on sulfur removal from liquid iron by hydrogen plasma arc melting. Modern Physics Letters B, 2021, 35, .	1.9	1
117	High Magnetic Field Processing of Metal Alloys. Springer Series in Materials Science, 2018, , 195-242.	0.6	0
118	Effects of axial static magnetic field on columnar to equiaxed transition in directionally solidified low carbon steel. Ironmaking and Steelmaking, 2020, 47, 398-404.	2.1	0
119	Evolution Mechanism of Microporosity of Nickel-Based Single-Crystal Superalloy During Solution Heat Treatment Under an Alternating Magnetic Field. Metallurgical and Materials Transactions B: Process Metallurgy and Materials Processing Science, 2021, 52, 30-35.	2.1	0